Large Tunneling Magnetoresistance and Perfect Spin Filtering Effect in van der Waals $Cu/FeX_2/h\text{-}BN/FeX_2/Cu$ (X = Cl, Br, I) Magnetic Tunnel Junctions

Xinlong Dong(董新龙)[1,2,3†], Xiaowen Shi(师小文)[1,2†], Dan Qiao(乔丹)[1,2], Zeyu Li(李泽宇)[3], Yuhao Bai(白宇浩)[1,2*], Zhenhua Qiao(乔振华)[3,4*], and Xiaohong Xu(许小红)[2*]

[1]*College of Physics and Information Engineering, Shanxi Normal University, Taiyuan 030031, China*
[2]*Key Laboratory of Magnetic Molecules and Magnetic Information Materials of the Ministry of Education, Research Institute of Materials Science, Shanxi Normal University, Taiyuan 030031, China*
[3]*International Center for Quantum Design of Functional Materials, University of Science and Technology of China, Hefei 230026, China*
[4]*Hefei National Laboratory, University of Science and Technology of China, Hefei 230088, China*

(Received 9 July 2024; accepted manuscript online 4 September 2024)

The two-dimensional magnetic van der Waals heterojunctions have opened unprecedented opportunities to explore new physics due to their potential for spintronic applications. Here, combing density functional theory with non-equilibrium Green's function technique, we systematically investigate the spin-polarized transport properties of $Cu/FeX_2/h\text{-}BN/FeX_2/Cu$ (X = Cl, Br, I) magnetic tunnel junctions (MTJs). It is found that the maximum tunneling magnetoresistance of $Cu/FeCl_2/h\text{-}BN/FeCl_2/Cu$, $Cu/FeBr_2/h\text{-}BN/FeBr_2/Cu$, and $Cu/FeI_2/h\text{-}BN/FeI_2/Cu$ MTJs can reach 3443%, 3069%, and 1676%, respectively. In the parallel state, the resistance area products at zero bias for $Cu/FeCl_2/h\text{-}BN/FeCl_2/Cu$, $Cu/FeBr_2/h\text{-}BN/FeBr_2/Cu$, and $Cu/FeI_2/h\text{-}BN/FeI_2/Cu$ MTJs are 0.92, 0.47, and $0.32\,\Omega{\cdot}\mu m^2$, respectively. More interestingly, our results indicate that $Cu/FeX_2/h\text{-}BN/FeX_2/Cu$ (X = Cl, Br, I) MTJs can realize spin filtering effect, while $Cu/FeCl_2/h\text{-}BN/FeCl_2/Cu$ and $Cu/FeI_2/h\text{-}BN/FeI_2/Cu$ MTJs exhibit negative differential resistance. Our results demonstrate that large tunneling magnetoresistance, negative differential resistance effect, low resistance area product as well as excellent spin filtering effect coexist in $Cu/FeCl_2/h\text{-}BN/FeCl_2/Cu$ and $Cu/FeI_2/h\text{-}BN/FeI_2/Cu$ MTJs, and that the feasible tunability of such a kind of van der Waals magnetic tunnel junctions is beneficial to designing next-generation logic devices.

DOI: 10.1088/0256-307X/41/10/107501

The discovery of large tunneling magnetoresistance (TMR) in the magnetic tunnel junctions has shown fascinating applications in spintronics, such as magnetic sensors, magnetic random access memory, and logic devices.[1–4] The tunneling magnetoresistance ratio is a critical factor in determining the merit of a device. So far, extensive theoretical and experimental efforts have been dedicated to developing magnetic tunnel junctions with various ferromagnetic metals and insulating materials to achieve a high tunneling magnetoresistance ratio, which is necessary for the successful implementation of magnetic tunnel junctions in practical applications. It is widely recognized that the tunnel barrier, a crucial element in a magnetic tunnel junction, is usually made up of metal oxides, such as MgO or Al_2O_3. However, ensuring precise control over barrier thickness while minimizing non-uniformity, pinholes, and point defects in these metal oxides presents substantial challenges. Furthermore, the resistance-area (RA) products of transition metal magnetic tunnel junctions are often relatively high. For the next-generation read head, a low resistance-area RA product is required to satisfy the impedance matching indispensable for high-speed readout. Fortunately, there is a growing interest in incorporating layered two-dimensional materials into magnetic tunnel junctions as a solution to these limitations and to enhance the overall device performance.[5]

Experimentally, the large-scale production of two-dimensional materials, as reported in several studies,[6–8] has allowed for their successful integration in magnetic tunnel junctions. For instance, they have already been incorporated into graphene devices to enhance spin-transport properties,[9,10] and have been used as barriers in van der Waals heterostructures and vertical devices.[11–13] Furthermore, two-dimensional van der Waals magnetic materials have garnered significant attention since the successful syntheses of atomically thin $Cr_2Ge_2Te_6$,[14] and Fe_3GaTe_2[15] flakes. Zhang *et al.* proposed to combine the magnetic element Cr and the non-magnetic element boron to design novel 2D magnetic systems.[16] Compared to transition metal magnetic tunnel junctions that consist of ferromagnetic electrodes and oxide barrier layers, it has been reported that magnetic tunnel junctions utiliz-

†These authors contributed equally to this work.
*Corresponding authors. Email: bhy198322@163.com; qiao@ustc.edu.cn; xuxh@sxnu.edu.cn
© 2024 Chinese Physical Society and IOP Publishing Ltd

ing two-dimensional magnetic layers demonstrate superior performance.[17–33]

Recently, $FeCl_2$ has been synthesized by molecular-beam epitaxy,[34] providing compelling evidence for ferromagnetism in monolayer $FeCl_2$ on Au(111) surfaces. Notably, a Curie temperature (T_c) of $\sim$147 K is revealed for monolayer $FeCl_2$.[35] Theoretically, it has been proposed that $FeCl_2$ functions as an intrinsic half-metallic ferromagnet.[36–38] Moreover, analogous ferromagnetic properties have been observed in $FeBr_2$ and FeI_2.[39,40] Inspired by these findings, we simulated magnetic tunnel junctions based on FeX_2(X = Cl, Br, I). We used h-BN as the barrier layer and FeX_2 (X = Cl, Br, I) as the ferromagnetic layer. They were stacked together by weak van der Waals forces, which formed FeX_2/h-BN/FeX_2 sandwich structures. By employing the non-equilibrium Green's function combined with density-functional theory, we systematically investigated the spin transport properties of Cu/$FeCl_2$/h-BN/$FeCl_2$/Cu, Cu/$FeBr_2$/h−BN/$FeBr_2$/Cu, and Cu/FeI_2/h-BN/FeI_2/Cu magnetic tunnel junctions (MTJs). The maximum TMR can reach 3443%, 3069%, and 1676% for Cu/$FeCl_2$/h-BN/$FeCl_2$/Cu, Cu/$FeBr_2$/h-BN/$FeBr_2$/Cu, and Cu/FeI_2/h-BN/FeI_2/Cu MTJs, respectively. Furthermore, a perfect spin filtering effect was observed in the Cu/$FeCl_2$/h-BN/$FeCl_2$/Cu, Cu/$FeBr_2$/h-BN/$FeBr_2$/Cu, and Cu/FeI_2/h-BN/FeI_2/Cu MTJs. Additionally, the negative differential resistance (NDR) effect was detected in both the Cu/$FeCl_2$/h-BN/$FeCl_2$/Cu and Cu/FeI_2/h-BN/FeI_2/Cu MTJs.

Computational Methods. All structural relaxation calculations were performed within the framework of density functional theory as implemented in the Vienna *ab initio* simulation package (VASP).[41,42] The electron-core interaction was described by the projected augmented wave[43,44] pseudopotential with the general gradient approximation (GGA) parameterized by Perdew, Burke, and Ernzerhof (PBE).[45] The electron wave function was expanded in plane waves up to a cutoff energy of 500 eV, and a $7 \times 7 \times 1$ Monkhorst–Pack k-grid[46] was used to sample the Brillouin zone of the supercell. The convergence criterion for the electronic energy was set to be 10^{-5} eV. The Hellman–Feynman force was smaller than 0.02 eV/Å in the optimized structure. A vacuum region of 20 Å was used in the structural relaxation calculations of the central regions to avoid interaction between adjacent slabs. Moreover, van der Waals force was considered through the DFT-D3 method in all structural optimizations.

The electronic transport properties were calculated by using the density-functional theory coupled with the nonequilibrium Green function[47] as implemented in the Nanodcal package.[48] The plane-wave cutoff energy was set to be 80 hartree. The double-ζ polarized atomic-orbital basis was used to expand all physical quantities.[49] In self-consistent calculation, the energy convergence criterion of Hamiltonian matrix was set to be 10^{-4} eV. More $50\times50\times1$ k-mesh points were set for calculating the spin-reversed current and transmission coefficients of all MTJs.

In the linear-response regime, the spin-polarized current I_σ and conductance G_σ are defined by the Landauer–Büttiker formula:[50,51]

$$I_\sigma = \frac{e}{h}\int T_\sigma(E)[f_{\rm L}(E) - f_{\rm R}(E)]dE, \tag{1}$$

$$G_\sigma = \frac{e^2}{h}T_\sigma, \tag{2}$$

where $\sigma = \uparrow, \downarrow$ denote the index of spin, e is the electron charge, h is Planck's constant, T_σ(E) is the spin-resolved transmission coefficient, and $f_{\rm L(R)}(E)$ are the Fermi–Dirac distribution functions of the left (right) electrode. The formula $I = I_\uparrow + I_\downarrow$ is used to calculate the total charge current I. The spin injection efficiency η can be calculated by

$$\eta = \left|\frac{I_\uparrow - I_\downarrow}{I_\uparrow + I_\downarrow}\right|. \tag{3}$$

In the equilibrium state, the η is estimated by using the transmission coefficient at the Fermi level.

The TMR value in the equilibrium state is calculated by[52]

$$\mathrm{TMR} = \frac{G_{\rm P} - G_{\rm AP}}{G_{\rm AP}} = \frac{T_{\rm P} - T_{\rm AP}}{T_{\rm AP}}, \tag{4}$$

and at bias voltages it can be expressed as[53]

$$\mathrm{TMR}_{(\rm V)} = \frac{(I_{\rm P} - I_{\rm AP})}{I_{\rm AP}} \times 100\%, \tag{5}$$

where $T_{\rm P/AP}$ and $I_{\rm P/AP}$ are the total transmission coefficient of the Fermi level and the currents in parallel and antiparallel states, respectively.

The resistance-area (RA) product at equilibrium can be calculated from transmission by definition[54]

$$\mathrm{RA} = \frac{\rm A}{\rm G} = \frac{\rm A}{T_{\rm (F)}G_0}, \tag{6}$$

at bias voltage V,[55]

$$\mathrm{RA}_{(\rm V)} = \frac{\rm VA}{I}, \tag{7}$$

where A is the unit cell area, $T_{\rm (F)}$ is the calculated transmission at the Fermi level, and $G_0 = \mathrm{e}^2/\mathrm{h}$ is the spin-conductance quantum, I is the current at bias voltage V.

Basic Properties of $FeCl_2$, $FeBr_2$ and FeI_2. A single layer of FeX_2 (X = Cl, Br, I) consists of monolayer Fe atoms sandwiched between two layers of X atoms. Figure 1(a) shows the top and side views of FeX_2 (X = Cl, Br, I). Initially, we conducted structure optimization for FeX_2, encompassing lattice constants and atomic positions. The optimized lattice parameters for $FeCl_2$, $FeBr_2$, and FeI_2 are 3.53, 3.74, and 4.02 Å, respectively, which are consistent with the previous theoretical values.[39] Next, to study the electronic properties of single-layer FeX_2, the band structures and density of state of single-layer FeX_2 are displayed in Figs. 1(b)–1(d). The majority spin channels keep semiconductor behavior with the band gaps of 4.43, 3.77, and 2.88 eV for $FeCl_2$, $FeBr_2$, and FeI_2, respectively. Nevertheless, the minority of spin channels pass through the Fermi level, and show metallic properties. Therefore, the band structures of $FeCl_2$, $FeBr_2$, and FeI_2 show half-metallic behavior. The total density of states and partial density of states for $FeCl_2$, $FeBr_2$, and FeI_2 are plotted in Figs. 1(b)–1(d). The asymmetry between the majority and minority

spin channels results in the magnetism of these systems, with magnetic moments of 4 μ_B. The states near the Fermi level are mainly formed by the Fe d orbitals, whereas a little X p (X = Cl, Br, and I) orbitals.

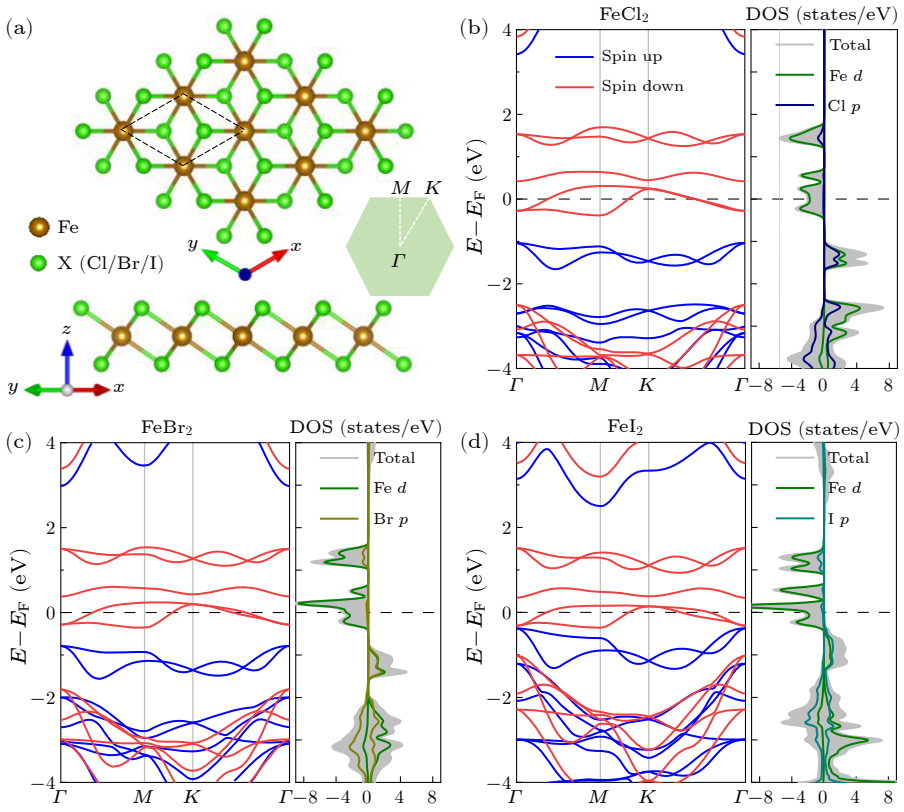

Fig. 1. (a) Top and side views of the FeX_2 (X = Cl, Br, and I). (b)–(d) Band structures and density of states of single-layer FeX_2 (X = Cl, Br, and I).

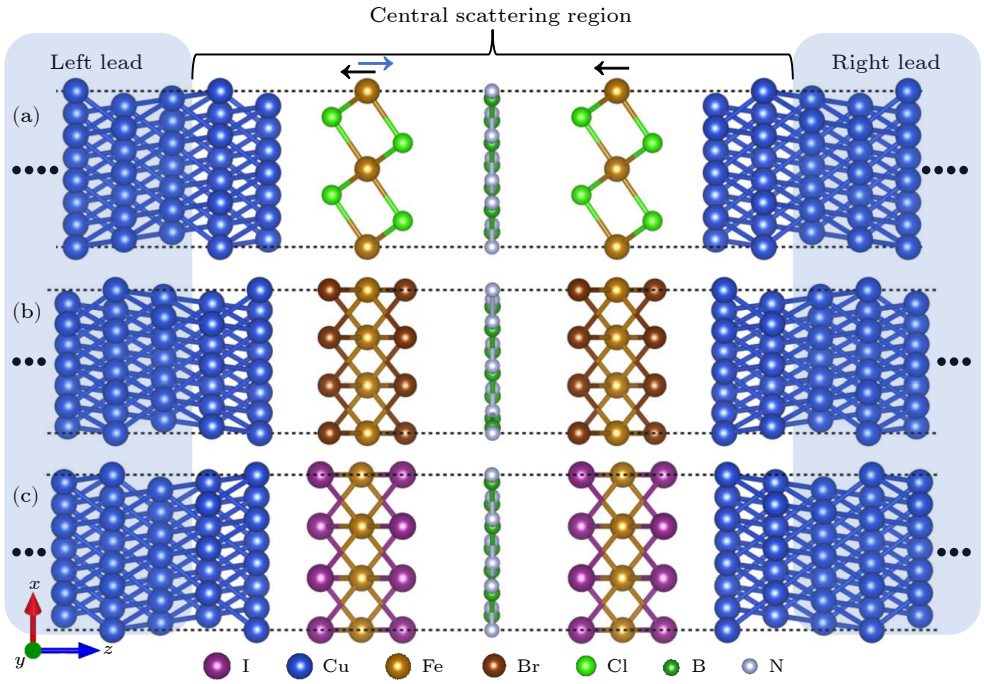

Fig. 2. Schematic of Cu/$FeCl_2$/h-BN/$FeCl_2$/Cu (a), Cu/$FeBr_2$/h-BN/$FeBr_2$/Cu (b), and Cu/FeI_2/h-BN/FeI_2/Cu (c) MTJs. These devices are periodic in the X and Y directions, and the current flows in the Z direction.

Spin Transport Properties of $Cu/FeCl_2/h$-$BN/FeCl_2/Cu$, $Cu/FeBr_2/h$-$BN/FeBr_2/Cu$, and $Cu/FeI_2/h$-$BN/FeI_2/Cu$ Magnetic Tunnel Junctions. Figure 2 displays our considered structure of $Cu/FeX_2/h$-$BN/FeX_2/Cu$, where we utilize h-BN as the barrier layer, and $FeCl_2$, $FeBr_2$ and FeI_2 as the ferromagnetic layers, respectively. The system is separated into three adjacent regions: the central scattering region, the left and right electrodes [i.e., Cu (111)], respectively. When constructing the central region, we consider three cases, namely $Cu/FeCl_2/h$-$BN/FeCl_2/Cu$, $Cu/FeBr_2/h$-$BN/FeBr_2/Cu$, and $Cu/FeI_2/h$-$BN/FeI_2/Cu$ MTJs. In the context of monolayer $FeCl_2$ ($FeBr_2$ or FeI_2) adjacent to h-BN, when the magnetic moments of Fe atoms are aligned the same direction, the system is considered to be in the parallel (P) state. Conversely, if the magnetic moments of Fe atoms are aligned in opposite directions, the system is said to be in the antiparallel (AP) state. Prior to the transport calculation, we perform optimization on the FeX_2/h-BN/FeX_2 structure in the central area and determine the optimal distance between the Cu electrode and the FeX_2 layer. The calculated results indicate that the optimized distances between the Cu electrode and $FeCl_2$, $FeBr_2$, and FeI_2 are 2.48, 2.73, and 2.63 Å, respectively.

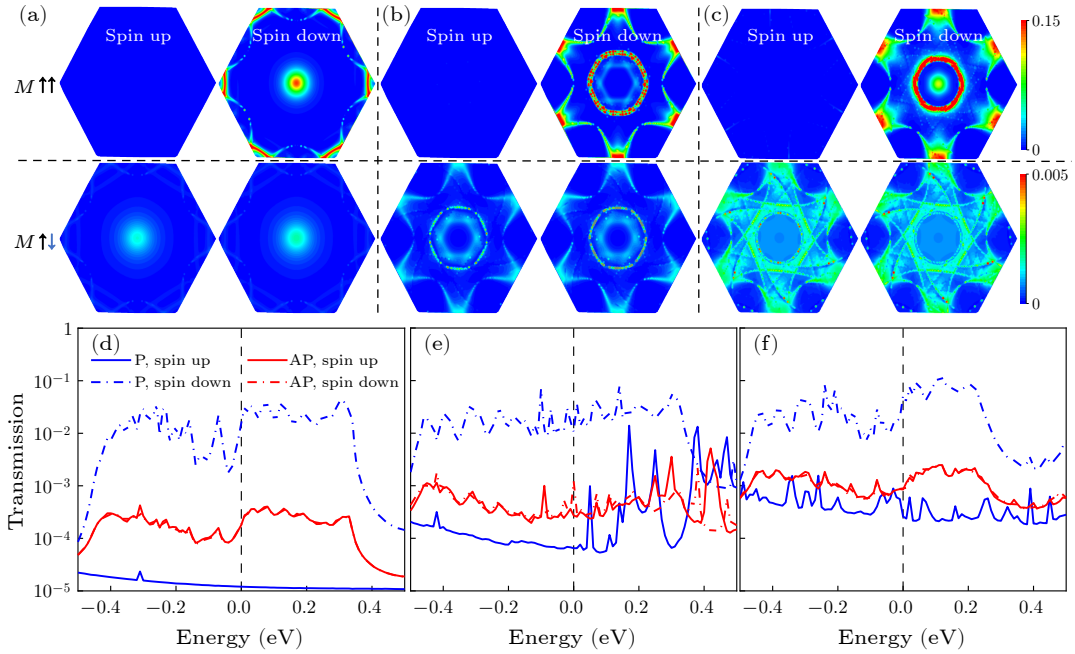

Fig. 3. The $k_\parallel$-resolved transmission coefficients across the $Cu/FeCl_2/h$-$BN/FeCl_2/Cu$, $Cu/FeBr_2/h$-$BN/FeBr_2/Cu$, and $Cu/FeI_2/h$-$BN/FeI_2/Cu$ MTJs [(a), (b), (c)] in the 2D Brillouin zone at the Fermi level. Transmission coefficients as a function of energy in the equilibrium state for $Cu/FeCl_2/h$-$BN/FeCl_2/Cu$, $Cu/FeBr_2/h$-$BN/FeBr_2/Cu$, and $Cu/FeI_2/h$-$BN/FeI_2/Cu$ MTJs [(d), (e), (f)]. In the antiparallel (AP) state, the red solid line denotes the spin-up state, while the red dashed line signifies the spin-down state.

To illustrate the influence of magnetization on electron transmission, we calculate the $k_\parallel$-resolved transmission coefficients of $Cu/FeCl_2/h$-$BN/FeCl_2/Cu$, $Cu/FeBr_2/h$-$BN/FeBr_2/Cu$, and $Cu/FeI_2/h$-$BN/FeI_2/Cu$ MTJs at the Fermi level in the 2D Brillouin zone as plotted in Figs. 3(a)–3(c). At the parallel state ($M_{\uparrow\uparrow}$), it can be observed that the "hot spots" are only present for spin-down channel, almost disappear for spin-up, which means a perfect spin filtering effect at the Fermi level. At the antiparallel state ($M_{\uparrow\downarrow}$), almost no "hot spots" are observed, indicating that the spin-up and spin-down channels are suppressed. As can be seen from the transmission coefficients in the equilibrium state in Figs. 3(d)–3(f), at the P state, it is apparent that there exists a noticeable spin polarization near the Fermi level, where the transmission coefficient of spin-down electrons exceeds that of the spin-up. However, at the AP state, the transmission coefficients of spin-up and spin-down are basically the same, compared to the P state, the value of the transmission coefficient is very small.

Next, we study the spin transport properties of $Cu/FeX_2/h$-$BN/FeX_2/Cu$ MTJs as a function of bias voltage by calculating I–V curves, tunneling magnetoresistance (TMR) and the spin injection efficiency η. Figures 4(a)–4(f) show the calculated I–V curves as a function of bias voltage ranging from -0.5 V to 0.5 V. At the P state, the total current is mainly contributed by the spin-down current, while the spin-up current is suppressed, thus the systems exhibit a perfect spin filtering effect. Therefore the $Cu/FeX_2/h$-$BN/FeX_2/Cu$ MTJs can be used as spin valves that the spin channel can be flexibly manipulated by applying magnetic field. For the P state of the $Cu/FeCl_2/h$-$BN/FeCl_2/Cu$ MTJ, with the increase of voltage, the spin-down current first increases up to a maximum

value at ±0.1 V, then decreases with the increase of voltage, exhibiting a negative differential resistance (NDR) effect. However, at the AP state, the current values for spin-up and spin-down are both extremely low, and almost inhibited in the bias range from −0.5 V to 0.5 V. In addition, the Cu/FeI_2/h-BN/FeI_2/Cu MTJ also exhibit significant negative differential resistance effect in the range of (0.3 V, 0.5 V) and (−0.3 V, −0.5 V). It is worth noting that the NDR effects for different magnetic configurations are different and are the most obvious for the P state, thus the NDR effects in these vdW MTJs can be modulated by applying electric field and magnetic field. The NDR effect has been widely used in electronic components such as frequency multipliers, memory devices, and fast switches. [56–60]

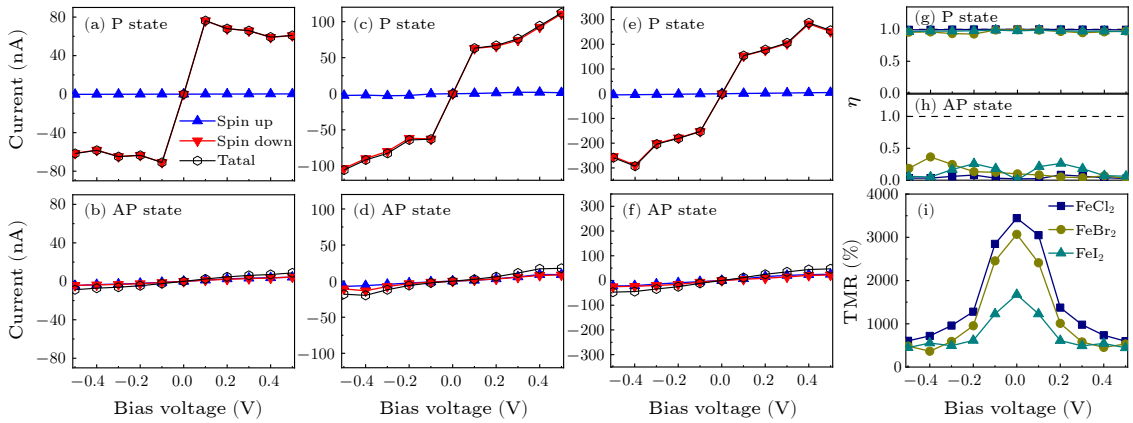

Fig. 4. (a)–(f) I–V curves, η [(g), (h)] and TMR (i) versus bias voltage of Cu/$FeCl_2$/h-BN/$FeCl_2$/Cu, Cu/$FeBr_2$/h-BN/$FeBr_2$/Cu, and Cu/FeI_2/h-BN/FeI_2/Cu MTJs.

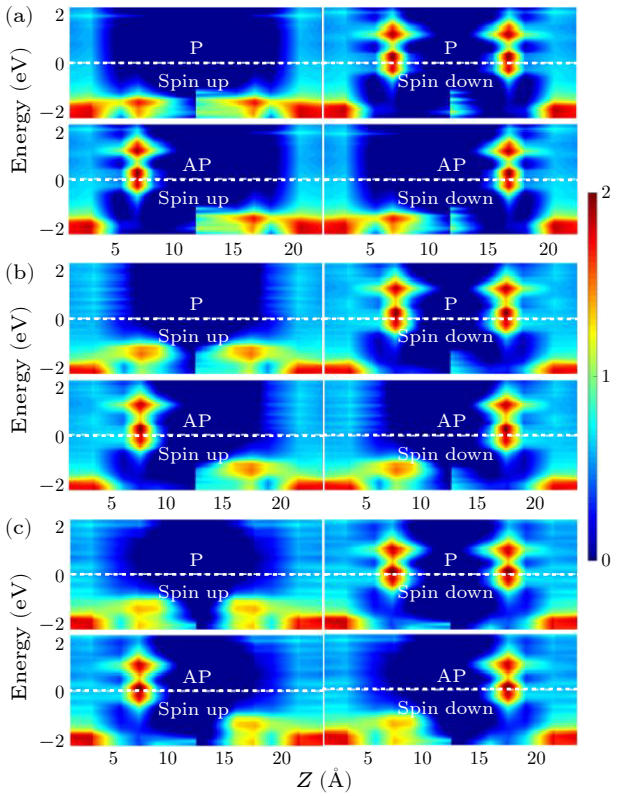

Fig. 5. Spin-resolved project density of states (PDOS) along the transport direction (z-axis) of the P and AP states of Cu/$FeCl_2$/h-BN/$FeCl_2$/Cu (a), Cu/$FeBr_2$/h-BN/$FeBr_2$/Cu (b), and Cu/FeI_2/h-BN/FeI_2/Cu MTJs (c).

We also plotted spin injection efficiency (η) as shown in Figs. 4(g) and 4(h). At the P state, the spin injection efficiency can be stabilized at 100% when the bias voltage ranging from −0.5 V to 0.5 V. Almost perfect spin filtering effects can be obtained for the P state of Cu/$FeCl_2$/h-BN/$FeCl_2$/Cu, Cu/$FeBr_2$/h-BN/$FeBr_2$/Cu, and Cu/FeI_2/h-BN/FeI_2/Cu MTJs. However, for the AP state, the spin injection efficiencies of all the three tunnel junctions are less than 50%. The TMR values of FeX_2 based MTJs are presented in Fig. 4(i). It is evident that, as the bias voltage increases, the TMR ratios decrease and reach their maximum values in the equilibrium state. The Cu/$FeCl_2$/h-BN/$FeCl_2$/Cu, Cu/$FeBr_2$/h-BN/$FeBr_2$/Cu, and Cu/FeI_2/h-BN/FeI_2/Cu MTJs exhibit maximum TMR ratios of 3443%, 3069%, and 1676%, respectively. If a magnetic tunnel junction has a tunneling magnetoresistance value exceeding 100%, it can be utilized in various applications such as magnetic field sensors, reading heads for hard drives, and magnetoresistive random access memories. [61–63] Therefore, the Cu/$FeCl_2$/h-BN/$FeCl_2$/Cu, Cu/$FeBr_2$/h-BN/$FeBr_2$/Cu, and Cu/FeI_2/h-BN/FeI_2/Cu MTJs can be considered as superior candidates to build spintronic devices.

To illustrate the spin-dependent transport properties, we present the real-space projected density of states (PDOS) for the MTJs consisting of Cu/$FeCl_2$/h-BN/$FeCl_2$/Cu, Cu/$FeBr_2$/h-BN/$FeBr_2$/Cu, and Cu/FeI_2/h-BN/FeI_2/Cu MTJs in Fig. 5. The dark blue zone with a diameter of approximately 12 Å represents the barrier layer composed of h-BN located at the central region. Hereafter, we take the Cu/$FeCl_2$/h-BN/$FeCl_2$/Cu MTJ as an example to illustrate the physical mechanism. As shown in Fig. 5(a), at the P state, in the spin-up channel, there are few states of $FeCl_2$ near the Fermi level

and a thicker barrier on both sides of h-BN, indicating a high resistance state. However, electrons in the spin-down channels are majority states near the Fermi level, which dominate the transport with a low resistance state. At the AP state, the electrons in spin-up (spin-down) channels flow from the left monolayer $FeCl_2$, then penetrate into h-BN with majority (minority) states, and then further flow into the right $FeCl_2$ with minority (majority) states, thus providing the MTJ with a high resistance state. The above analysis can also be directly applied to $Cu/FeBr_2/h\text{-}BN/FeBr_2/Cu$ and $Cu/FeI_2/h\text{-}BN/FeI_2/Cu$ MTJs, as displayed in Figs. 5(b) and 5(c).

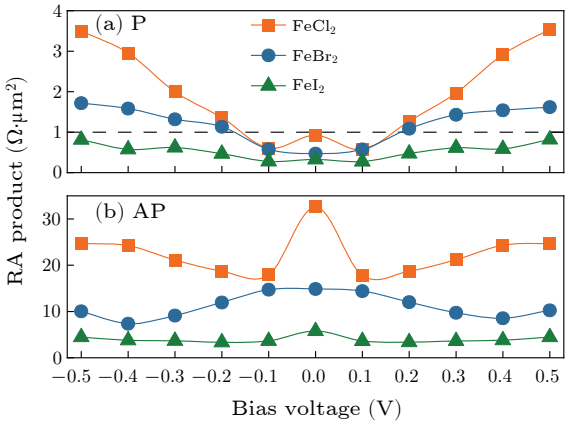

Fig. 6. Resistance area (RA) product as a function of bias voltage of the P (a) and AP (b) states for $Cu/FeCl_2/h\text{-}BN/FeCl_2/Cu$, $Cu/FeBr_2/h\text{-}BN/FeBr_2/Cu$, and $Cu/FeI_2/h\text{-}BN/FeI_2/Cu$ MTJs.

For the next-generation read head, a high tunneling magnetoresistance ratio is required to compensate for the reduction in the signal-to-noise ratio due to the shrinking recording bit size, and a low RA product is required to satisfy the impedance matching indispensable for high-speed readout. For example, when the recording density is $200\,\mathrm{Gbit/in^2}$, an RA product should lie bellow $1\,\Omega{\cdot}\mu m^2$. Figure 6 shows the variation of resistance area product with bias voltage under different magnetic configurations of the device. In the parallel state, the resistance area products at zero bias for $Cu/FeCl_2/h\text{-}BN/FeCl_2/Cu$, $Cu/FeBr_2/h\text{-}BN/FeBr_2/Cu$, and $Cu/FeI_2/h\text{-}BN/FeI_2/Cu$ MTJs are 0.92, 0.47, and $0.32\,\Omega{\cdot}\mu m^2$, respectively. By applying an external bias voltage, the minimum resistance area products for $Cu/FeCl_2/h\text{-}BN/FeCl_2/Cu$ and $Cu/FeI_2/h\text{-}BN/FeI_2/Cu$ are 0.565 and $0.272\,\Omega{\cdot}\mu m^2$, respectively. It is important to point out that $Cu/FeCl_2/h\text{-}BN/FeCl_2/Cu$ and $Cu/FeI_2/h\text{-}BN/FeI_2/Cu$ MTJs with high TMR, low RA product, NDR effect and excellent spin filtering effect, which are desirable performances for device applications.

In summary, we have systematically studied the electronic transport properties of $Cu/FeCl_2/h\text{-}BN/FeCl_2/Cu$, $Cu/FeBr_2/h\text{-}BN/FeBr_2/Cu$, and $Cu/FeI_2/h\text{-}BN/FeI_2/Cu$ MTJs using nonequilibrium Green's function and the density-functional theory. The TMR ratios in the equilibrium state are 3443%, 3069%, and 1676% for $Cu/FeCl_2/h\text{-}BN/FeCl_2/Cu$, $Cu/FeBr_2/h\text{-}BN/FeBr_2/Cu$, and $Cu/FeI_2/h\text{-}BN/FeI_2/Cu$ MTJs, respectively. More interestingly, the three devices all show nice spin filtering effect and low resistance area product. In addition, $Cu/FeCl_2/h\text{-}BN/FeCl_2/Cu$ and $Cu/FeI_2/h\text{-}BN/FeI_2/Cu$ MTJs show negative differential resistance effect, and the NDR effect in these vdW MTJs can be modulated by applying electric field and magnetic field.

Acknowledgements. This work was supported by the National Key Research and Development Program of China (Grant No. 2022YFB3505301), the Natural Science Basic Research Program of Shanxi (Grant No. 20210302124252), and the Innovation Project For Teaching Reform of Shanxi (Grant No. J20230616).

References

[1] Zhu J G and Park C 2006 *Mater. Today* **9** 36
[2] Heiliger C, Zahn P, and Mertig I 2006 *Mater. Today* **9** 46
[3] Chappert C, Fert A, and Van Dau F N 2007 *Nat. Mater.* **6** 813
[4] Wood R 2009 *J. Magn. Magn. Mater.* **321** 555
[5] Piquemal-Banci M, Galceran R, Caneva S, Martin M B, Weatherup R S, Kidambi P R, Bouzehouane K, Xavier S, Anane A, Petroff F, Fert A, Robertson J, Hofmann S, Dlubak B, and Seneor P 2016 *Appl. Phys. Lett.* **108** 102404
[6] Li X, Cai W, Colombo L, and Ruoff R S 2009 *Nano Lett.* **9** 4268
[7] Kim K K, Hsu A, Jia X, Kim S M, Shi Y, Hofmann M, Nezich D, Rodriguez-Nieva J F, Dresselhaus M, Palacios T, and Kong J 2012 *Nano Lett.* **12** 161
[8] Kidambi P R, Blume R, Kling J, Wagner J B, Baehtz C, Weatherup R S, Schloegl R, Bayer B C, and Hofmann S 2014 *Chem. Mater.* **26** 6380
[9] Yamaguchi T, Inoue Y, Masubuchi S, Morikawa S, Onuki M, Watanabe K, Taniguchi T, Moriya R, and Machida T 2013 *Appl. Phys. Express* **6** 073001
[10] Yankowitz M, Xue J, and LeRoy B J 2014 *J. Phys.: Condens. Matter* **26** 303201
[11] Geim A K and Grigorieva I V 2013 *Nature* **499** 419
[12] Britnell L, Gorbachev R V, Jalil R, Belle B D, Schedin F, Katsnelson M I, Eaves L, Morozov S V, Mayorov A S, Peres N M R, Castro Neto A H, Leist J, Geim A K, Ponomarenko L A, and Novoselov K S 2012 *Nano Lett.* **12** 1707
[13] Kamalakar M V, Dankert A, Bergsten J, Ive T, and Dash S P 2014 *Sci. Rep.* **4** 6146
[14] Gong C, Li L, Li Z, Ji H, Stern A, Xia Y, Cao T, Bao W, Wang C, Wang Y, Qiu Z Q, Cava R J, Louie S G, Xia J, and Zhang X 2017 *Nature* **546** 265
[15] Zha H, Li W, Zhang G, Liu W, Deng L, Jiang Q, Ye M, Wu H, Chang H, and Qiao S 2023 *Chin. Phys. Lett.* **40** 087501
[16] Zhang Y L, Zhang Y Y, Ni J Y, Yang J H, Xiang H J, and Gong X G 2021 *Chin. Phys. Lett.* **38** 027501
[17] Song T C, Cai X H, Tu M W Y, Zhang X O, Huang B, Wilson N P, Seyler K L, Zhu L, Taniguchi T, Watanabe K, McGuire M A, Cobden D H, Xiao D, Yao W, and Xu X D 2018 *Science* **360** 1214
[18] Zhang Y, Xu H, Feng J, Wu H, Yu G, and Han X 2021 *Chin. Phys. B* **30** 118504
[19] Li X L, Lü J T, Zhang J, You L, Su Y R, and Tsymbal E Y 2019 *Nano Lett.* **19** 5133
[20] Yan Z, Zhang R, Dong X, Qi S, and Xu X 2020 *Phys. Chem. Chem. Phys.* **22** 14773
[21] Pan L, Huang L, Zhong M, Jiang X W, Deng H X, Li J, Xia J B, and Wei Z 2018 *Nanoscale* **10** 22196
[22] Lin Z Z and Chen X 2020 *Adv. Electron. Mater.* **6** 1900968

[23] Zhang L, Li T, Li J, Jiang Y, Yuan J, and Li H 2020 *J. Phys. Chem. C* **124** 27429
[24] Zhou J, Qiao J, Duan C G, Bournel A, Wang K L, and Zhao W 2019 *ACS Appl. Mater. Interfaces* **11** 17647
[25] Pan L, Wen H, Huang L, Chen L, Deng H X, Xia J B, and Wei Z 2019 *Chin. Phys. B* **28** 107504
[26] Wu X M, Feng Y L, Li S, Zhang B Q, and Gao G Y 2020 *J. Phys. Chem. C* **124** 16127
[27] Feng Y L, Liu N, and Gao G Y 2021 *Appl. Phys. Lett.* **118** 112407
[28] Feng Y L, Wu X M, Hu L, and Gao G Y 2020 *J. Mater. Chem. C* **8** 14353
[29] Feng Y L, Wu X M, and Gao G Y 2020 *Appl. Phys. Lett.* **116** 022402
[30] Dong X, Jia X, Yan Z, Shen X, Li Z, Qiao Z, and Xu X 2023 *Chin. Phys. Lett.* **40** 087301
[31] Zhu W K, Xie S H, Lin H L, Zhang G J, Wu H, Hu T G, Wang Z A, Zhang X M, Xu J H, Wang Y J, Zheng Y H, Yan F G, Zhang J, Zhao L X, Patané A, Zhang J, Chang H X, and Wang K Y 2022 *Chin. Phys. Lett.* **39** 128501
[32] Lan G, Xu H, Zhang Y, Cheng C, He B, Li J, He C, Wan C, Feng J, Wei H, Zhang J, Han X, and Yu G 2023 *Chin. Phys. Lett.* **40** 058501
[33] Wang Z A, Zhang X M, Zhu W K, Yan F G, Liu P F, Yuan Z, and Wang K Y 2023 *Chin. Phys. Lett.* **40** 077201
[34] Zhou X H, Brzostowski B, Durajski A, Liu M Z, Xiang J, Jiang T R, Wang Z Q, Chen S W, Li P G, Zhong Z H, Drzewiński A, Jarosik M, Szczęśniak R, Lai T S, Guo D H, and Zhong D Y 2020 *J. Phys. Chem. C* **124** 9416
[35] Zhou X, Jiang T, Tao Y, Ji Y, Wang J, Lai T, and Zhong D 2024 *ACS Nano* **18** 10912
[36] Torun E, Sahin H, Singh S K, and Peeters F M 2015 *Appl. Phys. Lett.* **106** 192404
[37] Ceyhan E, Yagmurcukardes M, Peeters F M, and Sahin H 2021 *Phys. Rev. B* **103** 014106
[38] Ghosh R K, Jose A, and Kumari G 2021 *Phys. Rev. B* **103** 054409
[39] Kulish V V and Huang W 2017 *J. Mater. Chem. C* **5** 8734
[40] Ashton M, Gluhovic D, Sinnott S B, Guo J, Stewart D A, and Hennig R G 2017 *Nano Lett.* **17** 5251
[41] Kresse G and Hafner J 1993 *Phys. Rev. B* **48** 13115
[42] Kresse G and Furthmüller J 1996 *Comput. Mater. Sci.* **6** 15
[43] Blöchl P E 1994 *Phys. Rev. B* **50** 17953
[44] Kresse G and Joubert D 1999 *Phys. Rev. B* **59** 1758
[45] Perdew J P, Burke K, and Ernzerhof M 1996 *Phys. Rev. Lett.* **77** 3865
[46] Monkhorst H J, and Pack J D 1976 *Phys. Rev. B* **13** 5188
[47] Taylor J, Guo H, and Wang J 2001 *Phys. Rev. B* **63** 245407
[48] Taylor J, Guo H, and Wang J 2001 *Phys. Rev. B* **63** 121104
[49] Soler J M, Artacho E, Gale J D, García A, Junquera J, Ordejón P, and Sánchez-Portal D 2002 *J. Phys.: Condens. Matter* **14** 2745
[50] Meir Y and Wingreen N S 1992 *Phys. Rev. Lett.* **68** 2512
[51] Jauho A P, Wingreen N S, and Meir Y 1994 *Phys. Rev. B* **50** 5528
[52] Yuasa S, Nagahama T, Fukushima A, Suzuki Y, and Ando K 2004 *Nat. Mater.* **3** 868
[53] Parkin S S P, Kaiser C, Panchula A, Rice P M, Hughes B, Samant M, and Yang S H 2004 *Nat. Mater.* **3** 862
[54] Su Y, Li X, Zhu M, Zhang J, You L, and Tsymbal E Y 2021 *Nano Lett.* **21** 175
[55] Yadav M K and Gupta S K 2022 *Micro Nanostruct.* **165** 207192
[56] Rolf-Pissarczyk S, Yan S C, Malavolti L, Burgess J A J, McMurtrie G, and Loth S 2017 *Phys. Rev. Lett.* **119** 217201
[57] Perrin M L, Frisenda R, Koole M, Seldenthuis J S, Gil J A C, Valkenier H, Hummelen J C, Renaud N, Grozema F C, Thijssen J M, Dulić D, and van der Zant H S J 2014 *Nat. Nanotechnol.* **9** 830
[58] Rashidi M, Taucer M, Ozfidan I, Lloyd E, Koleini M, Labidi H, Pitters J L, Maciejko J, and Wolkow R A 2016 *Phys. Rev. Lett.* **117** 276805
[59] Dong Q X, Hu R, Fan Z Q, and Zhang Z H 2018 *Carbon* **130** 206
[60] Kuang G, Chen S Z, Yan L, Chen K Q, Shang X, Liu P N, and Lin N 2018 *J. Am. Chem. Soc.* **140** 570
[61] Duret C and Ueno S 2012 *NTN Tech. Rev.* **80** 64 (in Japanese)
[62] Mao S, Chen Y, Liu F *et al.* 2006 *IEEE Trans. Magn.* **42** 97
[63] Dave R W, Steiner G, Slaughter J M *et al.* 2006 *IEEE Trans. Magn.* **42** 1935